Nanostructured blazed gratings for high performance spectrographs

Simon Ans[a,b], Guillaume Demésy[b], Frédéric Zamkotsian[a], Andrei Mursa[c], Roland Salut[c], and Nicolas Passilly[c]

[a]Aix Marseille Univ, CNRS, CNES, LAM, Marseille, France
[b]Aix Marseille Univ, CNRS, Centrale Med, Institut Fresnel, Marseille, France
[c]FEMTO-ST, CNRS, UFC, Besançon, France

ABSTRACT

The state-of-the-art spectroscopy instruments are designed to collect as much light as possible, especially for astronomy applications. In this context, a blazed sub-wavelength disperser (called a metasurface) is a promising alternative to the widely used sawtooth blazed gratings with a metal coating. In order to find the optimal opto-geometric characteristics of such a device, topology optimization based on Finite Element modelling of Maxwell's equations is used. This paper deals with the application of this powerful optimization process, using different materials and introducing the manufacturability constraints. The reflection averaged on the [400,1500]nm wavelength range can reach 80% with a broadband optimization on silica. It is 28% higher than that of the sawtooth blazed grating (which reaches 52%) in absolute terms, and 54% in relative terms. First samples of metasurface gratings have been manufactured.

Keywords: Blazed gratings, Metasurface, Broadband optimization, Topology optimization, Maxwell's equations, Finite Element Method, e-beam lithography

1. INTRODUCTION

Spectroscopy is the keystone of Earth and Universe Observation. While imaging enables to study photometry and object morphology, spectroscopy is a crucial tool to access the composition of the space objects on the one hand, and their redshift z on the other hand. This is why spectro-imagers (or imaging spectrometers) are used in astronomy and constantly improved[1,2] . A special interest is expressed in the very device enabling the dispersion of light within the spectrograph: the blazed grating[3,4] . Several ways are explored to optimize its efficiency, using optical considerations such as in Ref. 2, 4 or with optimization methods, and more precisely topology optimization[5,6] .

This paper reports some applications of a homemade optimization code which is let open-source* and based on open-source softwares (Gmsh[7] and GetDP[8]). It relies on the resolution of the Maxwell's equations using the Finite Element Method (FEM) through a direct problem and an adjoint problem. The theory and illustrations of the method are gathered in Ref. 9. The goal of this presentation is to focus on the results and to have more in mind the impact of the manufacturability constraints. Therefore the choice of the material is discussed, as well as the shape of the optimal pattern, from a more practical point of view.

The section 2 introduces the theoretical geometry considered and the modelling tools used to optimize it with respect to the diffraction efficiency. The section 3 is dedicated to the topology optimization itself, and a focus is made on the initial configuration and the filters applied, particularly the binarization constraint. The section 4 is a description of the manufacturing method used for a pillar-shaped grating, made in parallel of the theoretical optimization to point out the manufacturability constraints and to optimize the methodology.

*https://gitlab.onelab.info/doc/models/-/tree/master/DiffractionGratingsTopOpt

2. THE DENSITY-DISTRIBUTION-BASED GRATING

Diffraction gratings are periodic structures that deflect an incident electromagnetic radiation to several directions, called diffraction orders which depend on the period, the wavelength and the angle of incidence. The diffraction efficiencies are the keystones of the study of such devices, since they provide the quantity of energy diffracted in each privileged direction. This quantity is especially intersting for blazed gratings. They are particular diffraction gratings that aim to scatter the incident electromagnetic field on one particular diffraction order.

We study here a mono-periodic blazed grating in reflection on the -1^{st} order. More precisely, we compare the common sawtooth profile (Fig. 1a) to a grating based on a distribution $\boldsymbol{\rho}$ of relative permittivities (Fig. 1b), also called a density distribution. On the one hand, the sawtooth grating is widely used in spectroscopy. On the other hand, the grating based on a density distribution of a given dielectric is inspired from the metasurfaces[10,11] : the dielectric is deposited on a flat layer of a reflective metal. It enables to avoid the resonances due to the sharp edges in the metal. Moreover, the preliminary optimization studies on this kind of grating detailed in Ref. 9 show that the metallic triangular pattern may be already close to the optimal one. The room for improvement is marginal.

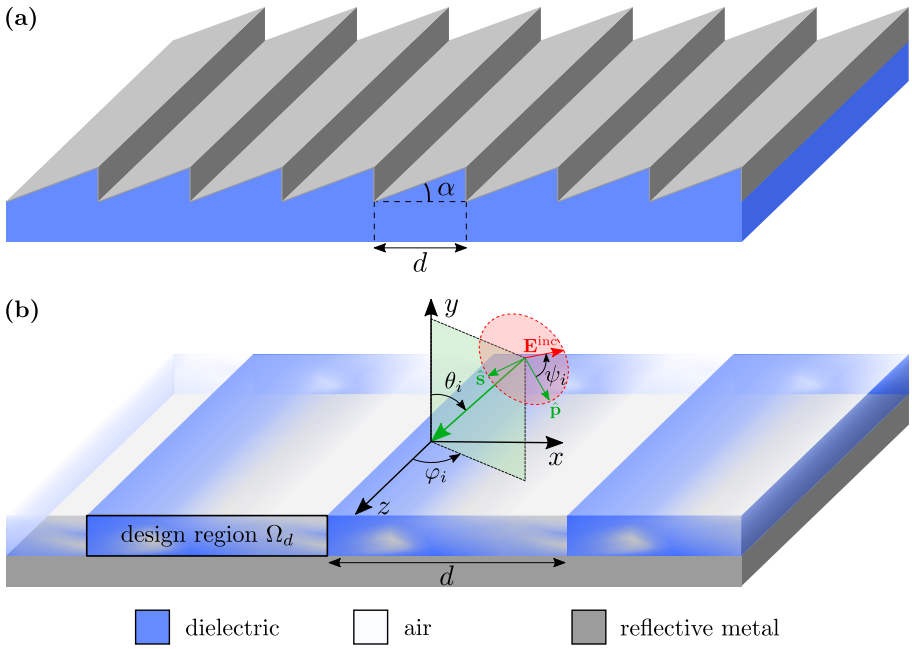

Figure 1. The two mono-periodic structures that are compared along this paper. Their period is the same and is denoted by d. The reflective metal for the considered range of wavelengths is silver Ag and the choice of the dielectric material is still to be done. **(a)** Sawtooth blazed grating in reflection. The angle α is called the blaze angle. **(b)** Mono-periodic grating based on a density distribution of relative permittivities. The design region Ω_d is highlighted. It corresponds to a period of the region containing the distribution of permittivities between that of air and that of the dielectric.

The modelling of the structure of Fig. 1b is detailed in Ref. 9. More particularly, the aim of the whole theoretical and numerical approaches is to access the diffraction efficiencies, only knowing the density distribution, the materials and the incident field. To that order, the resolution of the Maxwell's equations with the FEM is a key element. Once the efficiencies for all the orders n (R_n in reflection, T_n in transmission) are known, the goal is to optimize it on one paricular order. To that extent, topology optimization is used.

The FEM relies on the approximation of the continuous solution of a given Partial Differential Equation (PDE, here the Maxwell's equations) by a discrete solution on a mesh. This mesh is generated using Gmsh[7] . The resolution itself is ensured by the open-source software GetDP[8] and the optimization is based on the Globally Convergent Method of Moving Asymptotes (GCMMA)[12] taken over by the NLOpt[13] package.

3. TOPOLOGY OPTIMIZATION OF BLAZED GRATINGS

3.1 The Initial Configuration

For this study, the quantity R_{-1} is optimized on the wavelength range [400,1500] nm. This interval corresponds to nearly two octaves in the visible and Near InfraRed (NIR) ranges. The angles of incidence are $\theta_i = 5°$, $\varphi_i = -66°$ and $\psi_i = 90°$. As detailed in Ref. 9, topology optimization is a method based on the distribution of relative permittivities in the design region. The distribution is modified all along the optimization process in order to improve the target R_{-1}. Furthermore, two contraints of connectedness (no isolated elements that are too small) and binarization (the optimal pattern is made either of air or of dielectric) are added. The main hurdle of this approach is the calculation of the Jacobian of the target, which is ensured by the adjoint method. The theoretical results are obtained trough a demonstration similar as in Ref. 14.

The initial configuration is a distribution of relative permittivities that imitates the phase shift induced by the sawtooth grating. It is then a linearly decreasing density of permittivities, as illustrated on Fig. 2. For all that follows, if not specified, this configuration is used as the initial one for every optimization processes.

A last unknown is the thickness of this design region Ω_d. Let consider that the refractive index $n_{\text{diel}}(\lambda)$ of the dielectric material depends on the wavelength λ. Then the thickness of Ω_d should be

$$y_{\Omega_d}(\lambda) = \frac{d \tan \alpha}{n_{\text{diel}}(\lambda) - 1}. \tag{1}$$

It shows that the higher $n_{\text{diel}}(\lambda)$ is, the thiner Ω_d becomes. In order to let the most space possible in Ω_d, the chosen thickness is given by the equation (1) for the wavelength λ_* such as $n_{\text{diel}}(\lambda_*)$ is minimal in the wavelength range of interest.

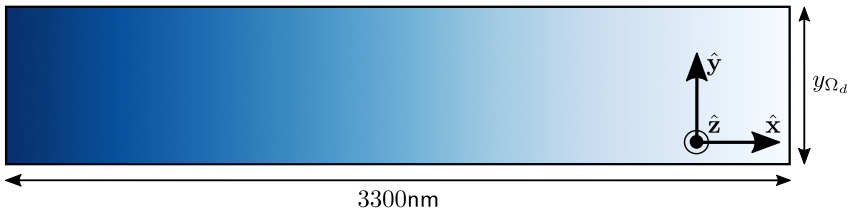

Figure 2. Initial distribution of relative permittivities in the period of the pattern. On the left, the density is of 100% (dielectric) and on the right, it is air. The period d is set to 3300 nm and the thicknes y_{Ω_d} depends on the dielectric material chosen, using Eq. (1).

3.2 Binarization and Connectedness Constraints

In order to obtain a readable optimal shape, there are two fundamental constraints. They may not be sufficient, but they are necessary to provide a pattern composed only with two materials (the *binarization* constraint) that are gathered in reasonably sized bundles (the *connectedness* constraint). For the binarization, the function applied to the permittivity distribution is:

$$\text{bin}(\boldsymbol{\rho}) = \frac{\tanh(\beta_m \nu) + \tanh[\beta_m(\boldsymbol{\rho} - \nu)]}{\tanh(\beta_m \nu) + \tanh[\beta_m(1 - \nu)]}, \tag{2}$$

where usually $\nu = 1/2$ and $\beta_m = 2^m$, with m increasing gradually during the optimization process. The connectedness constraint is a function that spreads a behaviour around a point (x, y) ($\rho(x, y)$ tending to 0 or 1) with a given radius r_f, which is here settled to 200 nm.

The combination of both contraints is illustrated on Fig. 3 on a specific input (Fig. 3a): 8 blurred rods that are too small for the connectedness radius. Three steps of binarization are displayed ($m = 3, 5, 7$, see Fig. 3b), as well as the effect of the sole connectedness contraint (Fig. 3c). The final constrained pattern (the output) is provided on Fig. 3d with $m = 7$ for the binarization.

For what follows, the dielectric settled is silica SiO_2[15] with $y_{\Omega_d} = 650$ nm. Let us first launch a monowavelength optimization of the -1^{st} diffraction order in reflection on the wavelength $\lambda = 700$ nm. At each step of

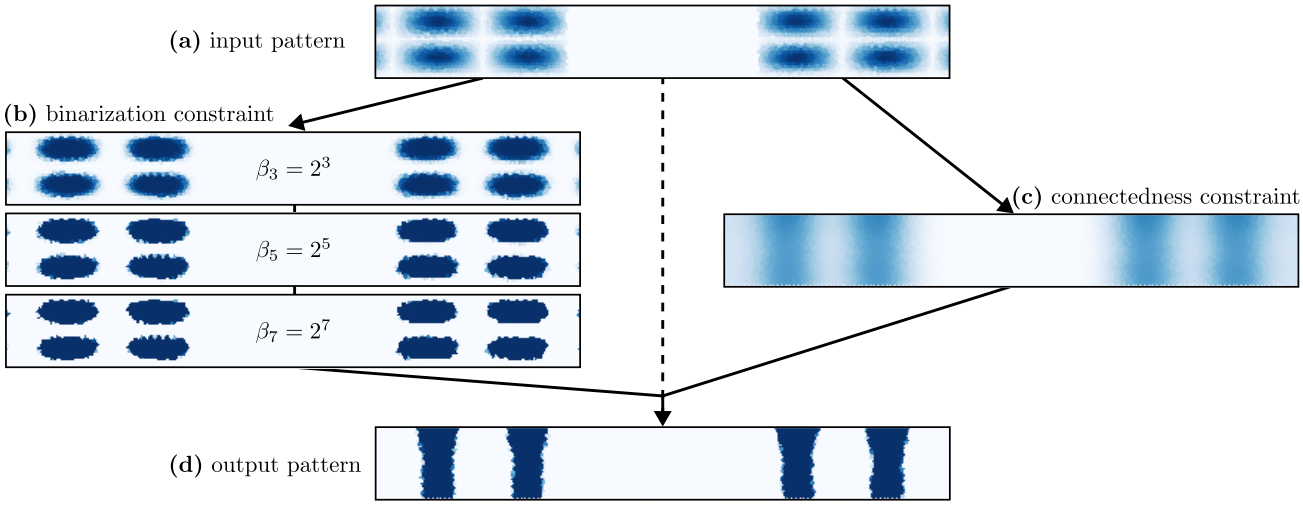

Figure 3. Binarization and connectedness process on the design region of Fig. 2 with $y_{\Omega_d}(\lambda) = 400\,\text{nm}$. **(a)** Let us consider an input pattern made of 8 blurred rods of size 300×150 nm. **(b)** The binarization constraint is the function described in Eq. (2) applied to the density field. It coerces gradually the permittivity distribution to a dielectric/air pattern. The blurr eventually vanishes. **(c)** The connectedness conntraint spreads the rods around their centers, gathering them by vertical couples. **(d)** The combination of both binarization ($m = 7$) and connectedness leads to four identical columns as an output (the differences are due to the finite element mesh).

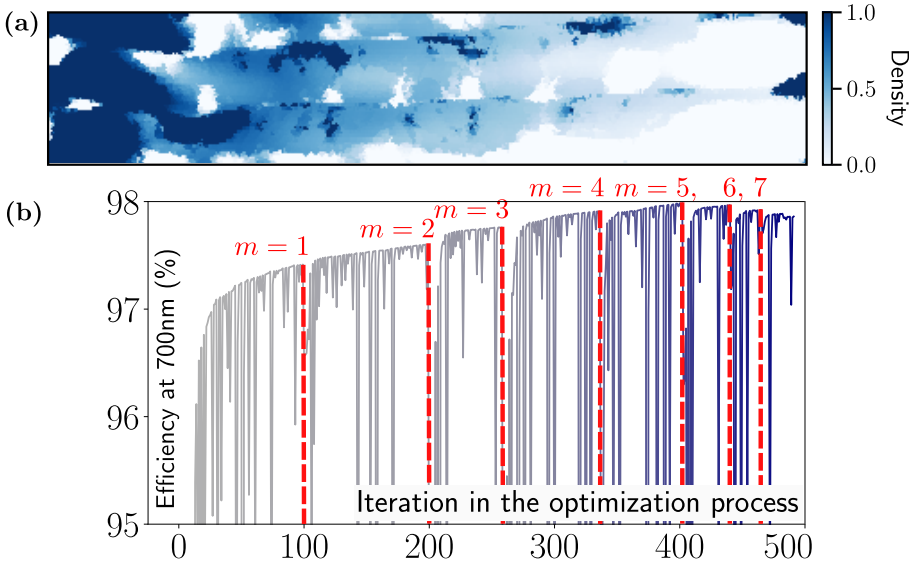

Figure 4. **(a)** Optimal pattern after the first step of the optimization process: $y_{\Omega_d} = 650\,\text{nm}$ of silica, $m = 1$ and $r_f = 200\,\text{nm}$ for the connectedness. **(b)** Evolution of the -1^{st} diffraction efficiency at 700 nm during the optimization process, zoom on the [95,98]% efficiency interval. Each drop corresponds to an increment of the binarization process m which are imposed at the red dashed lines.

the optimization process, strating from $m = 1$ (no binarization), both constraints are applied. Therefore, to begin with, the algorithm is looking for the optimal pattern regarding the targeted diffraction efficiency, only by looking for connected shapes. However, the obtained pattern after this first iteration of m is actually too blurry (see Fig. 4a). This is why m is gradually increased until a "full" binarization (settled to $m = 7$), finding each time an optimal pattern. It enables to better guide the algorithm to a high maximum, suggesting the binarized pattern step by step, as illustrated by the evolution of the target on Fig. 4b. The optimal diffraction efficiency found is led by the previous binarization iterations. After a small drop down when m is increased, the efficiency recovers a high value (nearly 100%). Finally, the last three binarization steps constraint the reflection

efficiency so much that it slightly decreases. However the fully binarized and optimized pattern enables to reach a diffraction efficiency on the -1^{st} diffraction order of 97.9%. This result is detailed in the next subsection, with the main optimization results on silica.

3.3 Topology Optimization on Silica

This preliminary study aims to control the optimization method. Does it enable to reach a 100% maximum on a single wavelength ? Is it possible to obtain a broadband pattern ? These questions find their answers by ignoring the manufacturing contraints in the first instance. The results are presented in Ref. 9 and are summarized on Fig. 5.

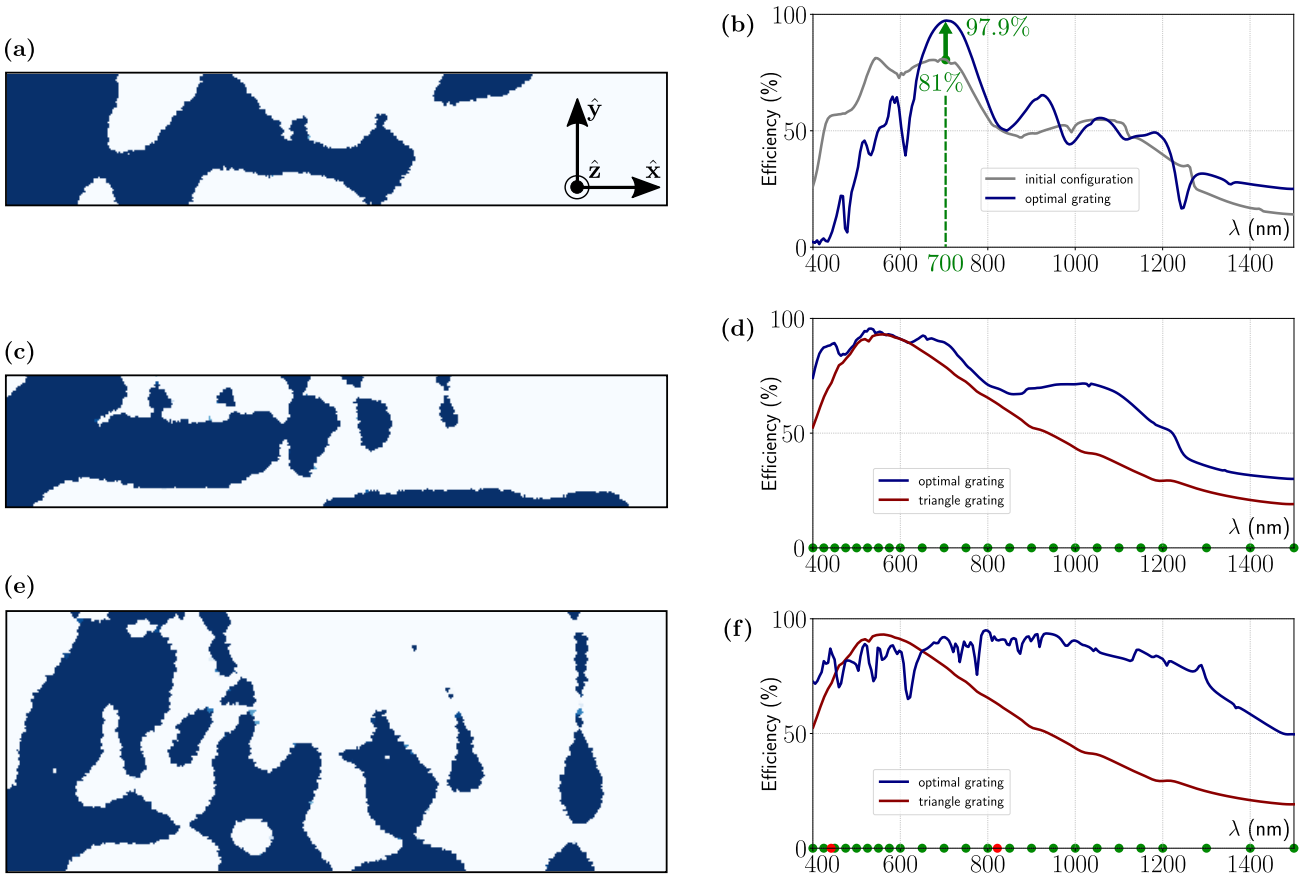

Figure 5. Optimization results on silica for two values of y_{Ω_d}, for a mono-wavelength and a broadband targeted diffraction efficiency. **(a)** Optimal pattern for a mono-wavelength optimization on $\lambda_t = 700\,\text{nm}$, $y_{\Omega_d} = 650\,\text{nm}$. **(b)** Spectral response on the -1^{st} diffraction order in reflection of this pattern (blue curve), under the targeted wavelengths. The grey curve is the spectral response of the initial configuration of Fig. 2. **(c)** and **(d)** Same analysis for a broandband optimization. The targeted wavelengths are displayed by the green dots on the abscissa of Fig. d. The red curve is the spectral response of the sawtooth grating recovered by a reflective metal layer of Fig. 1a. **(e)** and **(f)** Same analysis than c and d for $y_{\Omega_d} = 1300\,\text{nm}$. The two red dots point out a correction in the optimization process to avoid main resonances.

This study exhibits the fact that a mono-wavelength optimization provides a really high diffraction efficiency of 98% on the -1^{st} diffraction order (blue curve on Fig. 5b). Knowing that the loss by Joule effect due to the metal is of 1%, it means that only 1% of the incoming radiation is deflected on the other diffraction orders. It is an almost perfect structure for this wavelength. Nonetheless, the grating obtained is not broadband since the structure is resonant. There is no reflection at all at 400 nm and after 1250 nm, it is under 30%. This is why a broadband optimization is considered, by targeting several wavelengths at the same time.

Therefore, as displayed on Fig. 5d, a broadband optimization enables to obtain a better spectral response (blue curve) than the sawtooth grating recovered by a reflective metal layer centered in the visible range

(red curve, $\alpha = 5°$). The diffraction efficiency averaged over the wavelength range [400,1500] nm, defined as $\int_{400}^{1500} R_{-1}(\lambda)\,\mathrm{d}\lambda/(1500-400)$, reaches now 66%. It is relatively 27% better than the diffraction efficiency obtained with the sawtooth profile. It also shows the crucial role of the choice of the targeted wavelengths. With an increased number of targets in the higher frequencies (visible range), the broad resonant dips are removed.

Increasing the thickness of the design space enables to reach an even higher reflection efficiency averaged over the wavelength interval. It is possible to reach 80% without large resonances as displayed on Fig. 5f, after a correction (two added targets represented by the red dots). This last optimal pattern on Fig. 5e thus outperforms the sawtooth grating by 54% relatively, which is a huge step forward. This has now to be confronted to the manufacturability of such devices, and thus a preliminary work is presented in the next section.

However the connectedness constraint on such a large design space seems to have defaults. Moreover, the aspect ratio of a 1300 nm-thick nanostructure is truly high from an etching perspective, as illustrated in the next section dealing with the manufacturing of metasurfaces. This is why it would be preferable to work with a dielectric with a high refractive index ($n \geq 2$). Then y_{Ω_d} would be lower though inducing the same phase shift. Therefore the next step of the study is to process optimizations on dielectrics with a higher refractive index.

4. MANUFACTURING OF METASURFACES

In parallel of the theoretical optimization, the study of nanostructure etching is crucial since it enables to know the strengths and limits of the actual manufacturing. To begin with, the pattern displayed on Fig. 6 has been chosen as a test. Indeed, it is based on the same principle as the hypothetical pattern of Fig. 2 after two main changes:

- the gradation in terms of relative permittivity has been replaced by a gradation in terms of relative refractive index on a given surface. Therefore, instead of having a lower density, a smaller quantity of dielectric is kept on this surface. On the latter, at the end, the averaged refractive index is the same for both configurations;
- in the same given surface, if there is more dielectric than air, "negative" pillars (holes, the white squares at the left of the pattern Fig. 6) are considered, and "positive" pillars (actual dielectric pillars, the blue squares) are settled in the other way round.

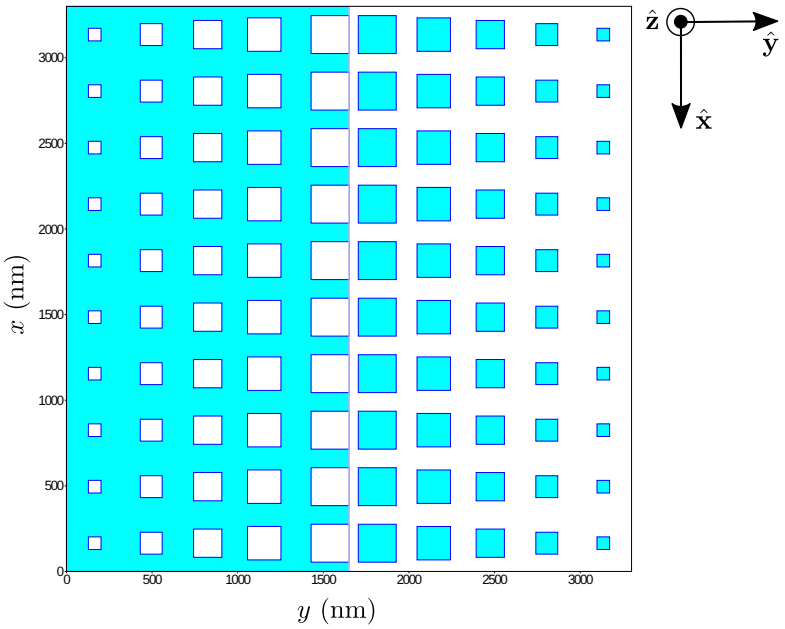

Figure 6. 3D pattern chosen for the etching preliminary study, view from above (as the configuration is now 3D, the basis has been changed). The dieletric is Nb_2O_5 and is represented by the blue surface.

The smallest pillars (negative or positive ones) have a size of 70 nm. A silica layer with a thickness of 1300 nm, or even 650 nm, leads thus to aspect ratios that are significantly high for this kind of geometry. This is why a dielectric with a higher refractive index is chosen: Nb_2O_5[16] .

To nanostructure this layer, we rely on electronic lithography in order first to expose a resin mask. It is then directly employed to transfer the pattern on the Nb_2O_5 layer using reactive-ion etching. The main issues are to reproduce the structure in an accurate as well as homogeneous way. For instance, a dependancy between the depth of the etching and the aspect ratio has to be avoided. This is why a stopping layer of aluminium oxide (50 nm of Al_2O_3) is deposited under the Nb_2O_5 one to protect the silver substrate.

Note that two layers of resin are deposited: an electro-sensitive one of 260 nm and a conductive one of 40 nm. The mask is baked a first time and then insolated using a locally adjusted e-beam lithography at low temperature (*RAITH Voyager* lithography system), and finally etched with C_2F_6 gas. The electronic dose chosen on every part of the cell of size 3.3 μm×3.3 μm represented on Fig. 6 notably depends on the surface to be insolated. By developing the resin, the whole structure is reproduced, as shown on the SEM view photograph on Fig. 7a.

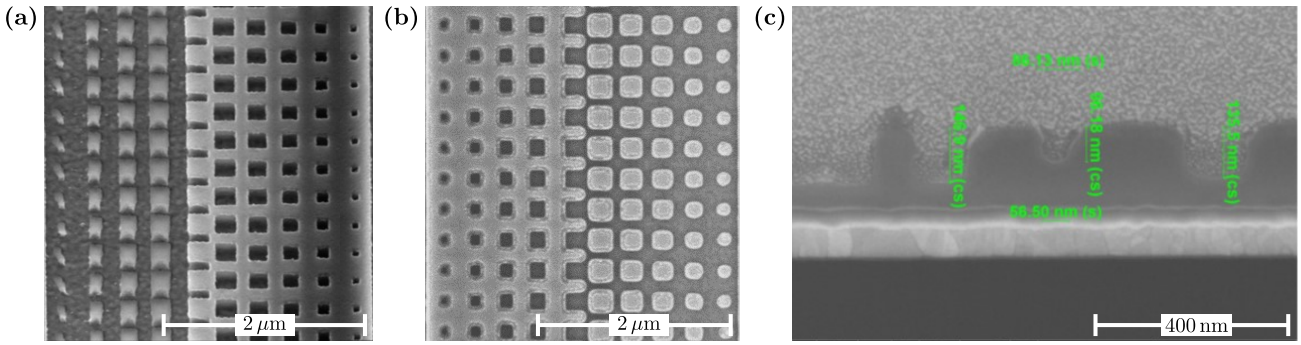

Figure 7. **(a)** Developed nanostrucured resin exposed by e-beam lithography. After several electronic dose tests, the whole structure is reproduced with the recquired dimensions. **(b)** SEM view of a cell after etching. The reproduction is really close to the pattern of Fig. 6, with curved edges. **(c)** Cross-section obtained through a FIB cut of the etched Nb_2O_5 structure. The etching depth is approximately of 150 nm.

The optimization of the process also aims to improve the selectivity of the etching, which is defined by how resisting the mask is regarding the actual material. However, Nb_2O_5 is hard to manufacture and the selectivity is only of 0.5 (while much improved). Before reaching the Al_2O_3 layer, the dielectric layer is attacked. The recquired pattern is truly well reproduced, however the edges of the pillars are curved (Fig. 7b), while a depth of approximately 150 nm is actually etched (Fig. 7c). A more tender material would likely lead to even more conclusing results. Combining these observations with a topology-optimized pattern is the next step of the project. Eventually, a totally controlled design and manufacturing chain is enabled trough it.

5. CONCLUSION

Topology optimization is a powerful tool for metasurface grating design. It provides promising results on mesh-based gratings, using the resolution of the Maxwell's equations with the Finite Element Method and the adjoint method.

A particular attention has been driven to the connectedness and binarization constraints on the pattern. Their actual effect has been illustrated on a simple example before their application to a more complete case. This application is a summary of the one developed in Ref. 9, with a theoretical diffraction efficiency reached 54% higher in relative terms than that of a grating with a sawtooth profil and a reflective metal coating. It is obtained on a pattern with a period $d = 3300$ nm and a thickness $y_{\Omega_d} = 1300$ nm.

Moreover, first samples of metasurface gratings have been manufactured using e-beam lithography. The etching of the dielectric material has been optimized on Nb_2O_5 and a precision of 70 nm-large by 150 nm-high has been reached. The performances of these samples will be characterized and the results will be compared to the models.

ACKNOWLEDGMENTS

The authors would like to thank CNES and Thales Alenia Space that partially fund this project with a PhD grant. Furthermore this work was supported by the French RENATECH network and its FEMTO-ST technological facility (MIMENTO). This part of the project has been partially funded by the CNRS PEPS-INSIS program through the project RESO-BATMAN.

REFERENCES

[1] M. Vachey, F. Zamkotsian, H. Benard, et al. "*MOEMS-based spectro-imagers for Earth and Universe Observation*". In *Proceedings of SPIE 11852, International Conference on Space Optics – ICSO 2020*, 2021.

[2] Z. Xiong, W. He, Q. Wang, et al. "*Design and optimization method of a convex blazed grating in the Offner imaging spectrometer*". *Appl. Opt.*, **60**(2):383–391, 2021.

[3] F. Zamkotsian, I. Zhurminsky, P. Lanzoni, et al. "*Blazed gratings on convex substrates for high throughput spectrographs for Earth and Universe Observation*". In *Proceedings of SPIE 11852, International Conference on Space Optics – ICSO 2020*, page 118520N, 2021.

[4] O. Sandfuchs, M. Kraus, and R. Brunner. "*Structured metal double-blazed dispersion grating for broadband spectral efficiency achromatization*". *J. Opt. Soc. Am. A*, **37**(8):1369–1380, 2020.

[5] B. Vial and Y. Hao. "*Open-source computational photonics with auto-differentiable topology optimization*". *Mathematics*, **10**(20):3912, 2022.

[6] J. Jiang, E. Lupoiu, E. W. Wang, et al. "*MetaNet: a new paradigm for data sharing in photonics research*". *Opt. Express*, **28**(9):13670–13681, 2020.

[7] C. Geuzaine and J. F. Remacle. "*Gmsh: a three-dimensional finite element mesh generator with built-in pre- and post-processing facilities*". *Int. J. for Numer. Methods Eng.*, **79**(11):1309–1331, 2009.

[8] P. Dular, C. Geuzaine, F. Henrotte, and W. Legros. "*A general environment for the treatment of discrete problems and its application to the finite element method*". *IEEE Trans. on Magn.*, **34**(5):3395–3398, 1998.

[9] S. Ans, F. Zamkotsian and G. Demésy. "*Topology optimization of blazed gratings under conical incidence*" (submitted). https://arxiv.org/abs/2403.10174, 2024.

[10] T. Phan, D. Sell, E. W. Wang, et al. "*High-efficiency, large-area, topology-optimized metasurfaces*". *Light: Sci. & Appl.*, **8**(48), 2019.

[11] Z. Li, R. Pestourie, Z. Lin, et al. "*Empowering metasurfaces with inverse design: principles and applications*". *ACS Photonics*, **9**(7):2178–2192, 2022.

[12] K. Svanberg. "*A class of globally convergent optimization methods based on conservative convex separable approximations*". *Soc. for Ind. Appl. Math.*, **12**(2):559–573, 2002.

[13] S. G. Johnson. The NLopt nonlinear-optimization package. https://github.com/stevengj/nlopt, 2007.

[14] E. Kuci, F. Henrotte, P. Duysinx, and C. Geuzaine. "*Combination of topology optimization and Lie derivative-based shape optimization for electro-mechanical design*". *Struct. Multidiscip. Optim.*, **59**(5):1723–1731, 2019.

[15] I. H. Malitson. "*Interspecimen comparison of the refractive index of fused silica*". *J. Opt. Soc. Am.*, **55**:1205–1208, 1965.

[16] F. Lemarchand. *Private communications* (2013). Measurement method described in:
L. Gao, F. Lemarchand, and M. Lequime. "*Exploitation of multiple incidences spectrometric measurements for thin film reverse engineering*". *Opt. Express*, **20**(14):15734–15751, 2012.